908–918 *Nucleic Acids Research, 2023, Vol. 51, No. 2* *Published online 30 December 2022*
https://doi.org/10.1093/nar/gkac1208

Polyribosomes of circular topology are prevalent in mammalian cells

Timur N. Baymukhametov[1], Dmitry N. Lyabin[2], Yury M. Chesnokov[3], Ivan I. Sorokin[2], Evgeniya V. Pechnikova[3,4], Alexander L. Vasiliev[3,4] and Zhanna A. Afonina[2,*]

[1]Structural biology department, National Research Center 'Kurchatov Institute', Moscow 123182, Russia, [2]Institute of Protein Research RAS, Pushchino, Moscow Region 142290, Russia, [3]Probe and Electron Microscopy Resource Center, National Research Center 'Kurchatov Institute', Moscow 123182, Russia and [4]Electron Microscopy Laboratory, Shubnikov Institute of Crystallography of Federal Scientific Research Centre 'Crystallography and Photonics' RAS, Moscow 119333, Russia

Received May 24, 2022; Revised December 02, 2022; Editorial Decision December 05, 2022; Accepted December 06, 2022

ABSTRACT

Polyribosomes, the groups of ribosomes simultaneously translating a single mRNA molecule, are very common in both, prokaryotic and eukaryotic cells. Even in early EM studies, polyribosomes have been shown to possess various spatial conformations, including a ring-shaped configuration which was considered to be functionally important. However, a recent *in situ* cryo-ET analysis of predominant regular inter-ribosome contacts did not confirm the abundance of ring-shaped polyribosomes in a cell cytoplasm. To address this discrepancy, here we analyzed the cryo-ET structure of polyribosomes in diluted lysates of HeLa cells. It was shown that the vast majority of the ribosomes were combined into polysomes and were proven to be translationally active. Tomogram analysis revealed that circular polyribosomes are indeed very common in the cytoplasm, but they mostly possess pseudo-regular structures without specific inter-ribosomal contacts. Although the size of polyribosomes varied widely, most circular polysomes were relatively small in size (4–8 ribosomes). Our results confirm the recent data that it is cellular mRNAs with short ORF that most commonly form circular structures providing an enhancement of translation.

INTRODUCTION

The majority of active mRNA molecules in the cell are typically translated by several ribosomes simultaneously, forming structures that topologically resemble a thread of beads. These dynamic complexes had been discovered even before the establishment of the main gene expression paradigm and named 'polyribosomes' or 'polysomes' (1–5).

Even in early electron microscopy studies, it was found that polyribosomes in eukaryotic cells can take a variety of shapes (3–13). Cytoplasmic polyribosomes were commonly described as a helical, double-row, or, most interestingly, a circular arrangement of ribosomes (3,8–12,14). This led to the assumption that each shape of polyribosomes reflects certain peculiarities of an mRNA translation. As early as 1965 it was first suggested that in circular polyribosomes mRNA chain forms a closed loop and ribosomes 'move along the circular mRNA without being released' (15). Later, functional studies revealed a slow exchange rate between translating polyribosomes and free cytoplasmic ribosomes, testifying that terminating ribosomal particles re-entry into the same translating polysomes (16,17). The model of circular mRNA translation was proposed, claiming that the proximity of mRNA 3′- and 5′-ends are important, allowing direct migration of ribosomes or ribosomal subunits from termination to initiation site (17).

Subsequently, the synergy between 5′ cap and 3′ poly(A) tail in promoting the translation of eukaryotic mRNAs was revealed, confirming that certain interaction between mRNA ends leads to translation enhancement (18,19). It was found that the continuous chain of RNA-protein and protein-protein interactions – 5′cap/eIF4E/eIF4G/PABP/3′poly(A) – bridges the mRNA termini together (20–23). Cap-to-poly(A) looping of free (non-polysomal) mRNA in the presence of initiation factors eIF4E, eIF4G, and PABP was demonstrated directly in atomic force microscopy experiments (24).

*To whom correspondence should be addressed. Tel: +7 985 7232812; Fax: +7 4967 318435; Email: afonina@vega.protres.ru
Present addresses:
Ivan I. Sorokin, Department of Virus-Cell Interactions, Belozersky Institute of Physico-Chemical Biology, Lomonosov Moscow State University, Moscow, 119234, Russia; Research Center for Molecular Mechanisms of Aging and Age Related Diseases, Moscow Institute of Physics and Technology, Dolgoprudny, Moscow Region 141701, Russia.
Evgeniya V. Pechnikova, Materials and Structural Analysis Division, Thermo Fisher Scientific, Achtseweg Noord, Eindhoven 5651 GG, The Netherlands.

Besides, the formation of eIF4F/PABP-mediated mRNA loops *in vivo* was detected recently (25).

These data pointed out an obvious conclusion, that it is the physical interaction of mRNA termini that provides the circularity of polyribosomes. However, it was shown that *in vitro* translation of RNA templates devoid of the cap, poly(A), or both led to the formation of circular polyribosomes in an amount close to that obtained upon translation of caped and polyadenylated mRNA (26). This result testifies that some other protein factors or ribosomes themselves can be involved in the formation of circular polyribosome structure.

Early EM data were obtained using traditional TEM approaches, where the preparation of a polyribosome sample involved contrasting with heavy metals and drying it on the EM grid (3,6–9). It was clear that such a harsh treatment may lead to a distortion of visible polysome morphology. For example, double-row polyribosomes visualized by conventional EM were commonly considered to be topologically circular, representing collapsed rings with opposite sides stuck together due to the drying of the sample (27,28). The observation that such polyribosomes formed in wheat germ cell-free system exhibited slow exchange with free ribosomes supported this belief (28).

Development of the cryoelectron tomography method (hereinafter, cryo-ET) allowed the study of the three-dimensional organization of polyribosomes quick-frozen in a thin layer of amorphous ice, avoiding staining and drying stages (26,29–33). Analysis of subtomograms with data processing methods allowed to achieve a resolution of 10–50 Å, depending on the sample (29,30,34). This resolution made it possible to determine the relative orientations of ribosomes with an accuracy sufficient to trace the path of the mRNA chain. Cryo-ET analysis of polyribosomes formed *in vitro* and interpreted on conventional TEM micrographs as double rows (28) showed that only part of them consisted of two anti-parallel chains of ribosomes, the rest are zig-zag-like forms that resemble double rows in traditional TEM micrographs (33). Also, a significant part of polyribosomes in these samples turned out to be three-dimensional helices with 4 ribosomes per turn that also look like double rows in two-dimensional images (33).

Besides studying polysomes formed *in vitro*, several attempts of *in situ* cryo-ET analysis of the structure of eukaryotic cytoplasmic polyribosomes were carried out (30,35,36). In the first study where detailed characterization of polyribosome organization *in situ* was made, the authors analyzed the distribution of ribosomes in protrusions of human glioma cells trying to determine the most represented regular shapes of polyribosomes (30). Interestingly, the preferable topology of the polyribosomes was predicted to be linear with a helical or spiral path of mRNA chain, and it was pointed out that the organization of polyribosomes resembles that in prokaryotes and that no direct evidence was found that supported the circular translation hypothesis (30). It is likely, though, that topologically circular polyribosomes were not detected because of the limitations of the approach used. Since the visual assignment of ribosomes to individual polysomes was difficult in tomograms due to the tight arrangement of ribosomes in the cytoplasm, identification of polyribosome morphology was based on the statistical analysis of predominant inter-ribosomal contacts. Thus, only polyribosomes featuring strictly ordered organization were detected, that is not typical for loosely packed circular polysomes of arbitrary shape (26). Another potential reason why circular polyribosomes were not detected in human glioma cells, is that in highly specialized cells such as neurons or other cells of nervous tissue linear polyribosome topology may be the prevalent one (30,35,36).

Here, we conducted a detailed cryo-ET study of the structural organization of cytoplasmic polyribosomes in diluted HeLa cell lysates. A significant distance between the individual polyribosomes in the sample allowed us to identify them reliably and determine their morphology. The most promising result is that a significant amount of topologically circular polyribosomes has been detected, which is, so far, the only cryo-EM evidence of their presence in the cytoplasm of eukaryotic cells. Besides, topologically linear helical, helix-like and zig-zag ribosome arrangements, as well as polyribosomes of random shape were identified in the lysate.

MATERIALS AND METHODS

Preparation of HeLa lysate by osmotic or detergent lysis

HeLa cells were cultivated on 10 cm dishes in DMEM/F12 supplemented with 10% fetal calf serum, 2 mM glutamine, 100 U/ml penicillin and 100 μg/ml streptomycin. The cells were incubated at 37°C in a humidified atmosphere containing 5% CO_2 and passaged by standard methods. When a cell line reached about 80% confluence, cycloheximide was added to the medium to the final concentration of 0.1 mg/ml and cells were incubated for 5 min at 37°C. Then the dish was transferred on ice and washed twice with cold PBS containing 0.1 mg/ml cycloheximide. 500 μl of osmotic lysis buffer (20 mM HEPES–KOH pH 7.6, 10 mM KCl, 5 mM $MgCl_2$, 0.1 mg/ml cycloheximide, 1 mM DTT, 1× Complete protease inhibitor without EDTA (Roche)) was added to the cells. Alternatively, cells were lysed with the same amount of Triton X-100 buffer (1% Triton X-100, 300 mM NaCl, 20 mM HEPES–KOH pH 7.6, 15 mM $MgCl_2$, 1 mg/ml heparin, 0.1 mg/ml cycloheximide, 1 mM DTT). The cells were incubated with lysis buffer for 2 min and collected into the Eppendorf tube by scraping. The RNAse inhibitor RiboLock (Thermo Fisher Scientific) was added to the lysate to the final concentration of 0.1 U/μl. The lysate was passed through a needle 27G (5 times) and the debris was removed by centrifugation for 5 min at 5000 × g and 4°C.

Puromycin test

HeLa cells were cultivated as described above until 80% confluence was reached. Puromycin was added to the medium instead of cycloheximide to the final concentration of 1 mM, cells were incubated for 10 min at 37°C. Further, the lysate was prepared by osmotic lysis in the same way as described above, but puromycin was added to PBS and lysis buffer instead of cycloheximide to the final concentration of 1 mM.

Analysis of HeLa lysate by sucrose gradient sedimentation

Preparation of gradients and sedimentation analysis were carried out as described earlier (28) besides the volume of the samples (HeLa lysate) loaded onto gradient was 100 μl.

Sample preparation for cryo-EM analysis

HeLa lysate sample was mixed with gold nanoparticle solution (10 nm Colloidal Gold Labeled Protein A, UMC Utrecht, Netherlands) in a ratio of 5:1, and 3 μl of the sample was applied to a glow-discharged (30 s, 25 mA) Quantifoil R2/2 300 mesh EM grid. After blotting for 0.5 s at 20°C and 100% humidity (blot force –7), the grid with the specimen was plunge-frozen into liquid ethane in Vitrobot Mark IV (Thermo Fisher Scientific, Hillsboro, OR, USA).

Cryoelectron tomography

The study was carried out at an accelerating voltage of 300 kV with a Titan Krios 60–300 TEM/STEM cryoelectron microscope (Thermo Fisher Scientific, USA), equipped with a Schottky-type field emission electron gun (FEI XFEG, the Netherlands), a spherical aberration corrector (CEOS GmbH, Germany), a CMOS-based Falcon II direct electron detector (Thermo Fisher Scientific, USA) and installed at NRC 'Kurchatov Institute' in Moscow, Russia. 40 tilt-series of the sample were collected automatically with Tomography software (Thermo Fisher Scientific, USA) in low-dose mode with 18 000 × nominal magnification (calibrated pixel size 3.7 Å) and the defocus value in the range between −3.0 and −4.5 μm using the bidirectional tilt scheme with tilt range ±60° at 2° increment. The cumulative dose was 61 $e^-/Å^2$ (∼1 $e^-/Å^2$ per single image).

Tomogram reconstruction

Cross-correlation alignment and tomographic reconstruction were performed using the IMOD (version 4.9.10, University of Colorado, Boulder, CO, USA) software package (37) by the simultaneous iterative reconstruction technique (SIRT) and weighted back-projection (WBP) method (38). Gold nanoparticles were used as fiducial markers for the alignment of the tilt-series projection images. Thirty six tilt-series with the alignment error not exceeding 1 pixel were selected for further processing. The reconstructions obtained by SIRT were used for visual inspection and particle picking, while the WBP reconstructions were used for subtomogram averaging.

Subtomogram averaging

The coordinates of 2976 ribosomes in polyribosomal complexes ('subtomograms') were manually picked from tomographic sections with IMOD and utilized for *de novo* reconstruction in Relion 2.1 (University of Cambridge, UK) (39) using subtomogram averaging (protocol described in (40)). The 3D CTF model was obtained for each of the subtomograms based on the defocus value estimated with CTFFIND4 (41). To ignore the signal from neighboring ribosomes, a soft mask was used. To reduce computing time binned tomograms were used for the averaging (binning factor 2, box size 64 × 64 × 64 px) which resulted in a 17.6 Å resolution, as determined by the Fourier Shell Correlation (FSC) 0.143 criteria (42,43). The map analysis showed that A- and P-sites are occupied with tRNAs, while focused 3D classification did not reveal any alternative tRNA positioning. Graphics and final visualization were performed with UCSF Chimera (44).

Single particle analysis

Single particle analysis of polysomal ribosomes was performed using the same samples after tilt-series data collection. A total of 500 movie-stacks (24 frames per stack) with the same 18 000 × nominal magnification (calibrated pixel size 3.7 Å) and the same total dose of 61 $e^-/Å^2$ (∼2.5 $e^-/Å^2$ per single frame) were collected automatically using EPU software (Thermo Fisher Scientific, USA). Drift correction using 5 patches, dose-weighting, per-frame local CTF estimation, as well as automated particle picking using a re-trained deep learning-based BoxNet method, were performed with Warp software (45). Reference-free 2D classification, *ab-initio* reconstruction, and map refinement were done using cryoSPARC v3.2 software (46). The final particle count after several rounds of 2D classification was 10408. The final resolution was estimated to be 7.7 Å using the 0.143 FSC criteria, which is close to the Nyquist frequency for a given pixel size. The classification did not reveal new structural states which would differ significantly in the presence or position of tRNAs from the consensus map.

RESULTS

Preparation of HeLa cell lysate suitable for the analysis of polyribosomes

For reliable discrimination and analysis of individual polyribosomes formed *in vivo*, it is necessary to prepare samples with a ribosome concentration substantially lower than that in the cytoplasm of the cell. Therefore, the preparation of diluted cell lysates becomes the cornerstone of the structural study of polyribosomes. The most common method to prepare mammalian cell lysates with intact polyribosomes is the lysis of cultured cells by a significant concentration of mild detergent (for example, 1% Triton X-100, (47)). Unfortunately, this method is not suitable for cryo-ET analysis, since the presence of the detergent substantially reduces the contrast of cryo-EM images (48). Therefore, we used osmotic shock as an alternative gentle method for cell lysate preparation. HeLa cell lysates were prepared by osmotic lysis, as well as by Triton X-100 treatment, and analyzed by fractionation in the sucrose gradient (Supplementary Figure S1A). The analysis of both preparations revealed a very similar shape of polysome distribution, pointing out that the lysates are similar, at least in terms of polyribosome quantity and size. Most of the ribosomes were detected in polysomal fractions (two or more ribosomes per mRNA) with a relatively small amount of monosomes and ribosomal subunits. The addition of puromycin to the cells before the lysis led to almost complete dissociation of the polysomes (Supplementary Figure

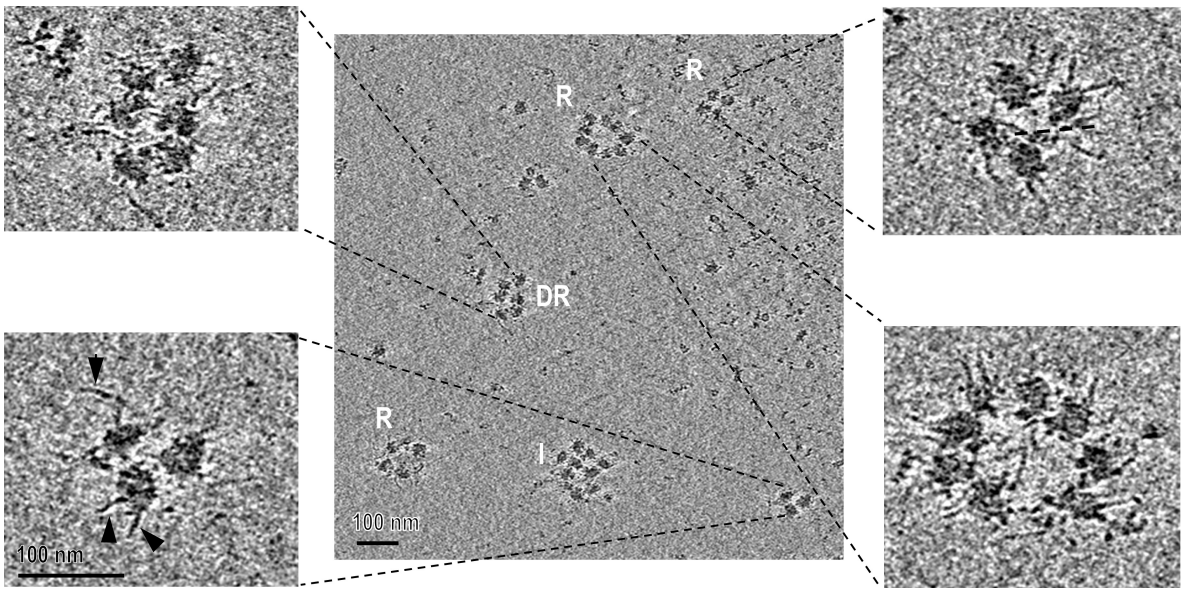

Figure 1. Cryo-ET analysis of a diluted HeLa lysate sample. Inserts represent the enlarged fragments with ribosome arrangements attributed to polysomes. Ring (R), double-row (DR) and indefinite shape (I) polyribosomes can be distinguished on the longitudinal section of the reconstructed tomogram. Arrows indicate flexible rRNA expansion segments (ES). Scale bars, 100 nm.

S1B) proving, that most of the polyribosomes were translationally active prior to the isolation from the cells. All these data confirm that the osmotic lysis is an appropriate method for preparing samples suitable for the analysis of polyribosomes.

Cryo-ET analysis of HeLa cell lysate: reliable determination of polyribosome morphology

Cryoelectron tomography makes it possible to study large heterogeneous complexes, such as polyribosomes, and to obtain structural data of reasonable quality. Cryo-ET allows solving the structure of individual polyribosomes under conditions close to native with a resolution sufficient to determine the mutual orientation of polysomal ribosomes. Earlier, we successfully used the method to analyze the structure of eukaryotic polyribosomes formed *in vitro* (26,31–33). The prospect of exploring the structural organization of polysomes in cell lysates has previously been demonstrated using prokaryotic *E. coli* lysates (29).

Freshly prepared HeLa cell lysate applied to an EM grid was flash-frozen in liquid ethane. The parameters of sample blotting were chosen so that the thickness of the amorphous ice layer was about 100 nm. The analysis of polyribosomes distribution through the thickness of tomograms revealed that the majority of medium size polyribosomes were inside the ice layer and the interactions with the ice surface were observed rarely. Thus, 3D configuration of polyribosomes was not significantly affected by surface tension effects. Tilt series images of HeLa lysate samples were acquired and reconstructed into 3D tomograms. In the longitudinal sections of the tomograms, individual polyribosomes of a ring, double-row or indefinite shape can be easily distinguished (see Figure 1 as an example). Interestingly, multiple rRNA expansion segments emerging from ribosomes are clearly seen in the sections. These flexible segments are characteristic of eukaryotic ribosomes, and the fact that they can be perceived in the tomograms indicates that the achieved resolution of the reconstruction was rather high.

To determine the topology of polyribosomes, we used a subtomogram technique which involves solving the averaged structure of the polysomal ribosome from the corresponding parts of the whole tomogram electron density map and inserting it into tomograms at proper positions (26,31–33,49). The ribosome was considered to be a part of a polysome if it had a neighbor at a distance not exceeding the characteristic size of the monosome. The subvolumes of the density map containing all 2976 visually identified polysomal ribosomes were extracted from the tomograms and subjected to best alignment with each other and to resulting averaging, giving both, the relative orientation of ribosomes and the averaged ribosome density map of about 17.6 Å resolution (Figure 2A). This resolution allowed us to discern not just the major characteristic features of ribosome structure (head and body of the 40S subunit, the central protuberance of the 60S subunit), but also smaller details, like tRNA molecules (Figure 2B). The presence of tRNA densities in A- and P-sites indicated that most of the polysomal ribosomes were in a translationally active state. The resulting average ribosome density was placed into the tomograms in positions and spatial orientations determined for each ribosome in the course of the alignment procedure, giving the 3D maps of all the polysomal ribosomes within the tomograms (Supplementary Figure S2). Only the polysomes with a size greater than 3 were taken into account since ribosome dimers and trimers can be considered as the initial elements in the formation of the polysome of any structural organization, circular, zig-zag or helical.

To clarify the position of tRNAs in polysomal ribosomes, we performed single particle analysis of the same frozen

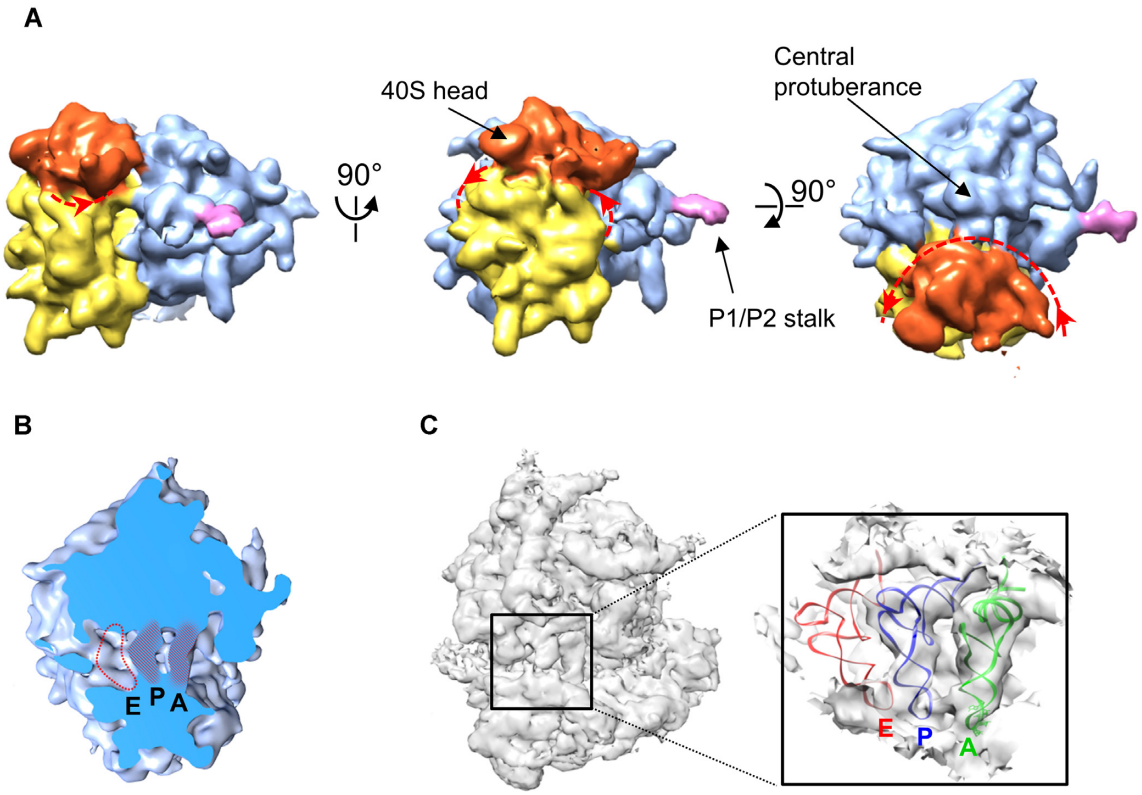

Figure 2. Cryo-EM structure of translating HeLa 80S ribosome. (**A**) Result of subtomogram averaging. 3D tomogram fragments containing individual polysomal ribosomes were extracted, aligned, and averaged, giving the structure of translating ribosome at 17.6 Å resolution. The head of the 40S ribosomal subunit is dyed in red and the body is in yellow, the 60S subunit is in blue with a pink P1/P2 stalk. The mRNA entry and exit sites are indicated with red dotted lines, arrowheads indicate the 3′ to 5′ direction of the mRNA chain. (**B**) The crosscut showing the presence of A-site and P-site tRNA densities (hashed areas) in the averaged ribosome subtomograms. The dotted line marks the expected position of the absent E-site tRNA. (**C**) 7.7 Å structure of translating HeLa 80S ribosome obtained by conventional single particle cryo-EM analysis. The insert represents the crosscut slice visualizing the electron densities corresponding to A-site (green) and P-site (blue) tRNA models positioned in pre-translocation A-A and P-P states, respectively. No tRNA density was detected in the E-site (red model). tRNA models were fitted into the 80S map according to PDB 5AJ0 (50) for P- and E-site tRNAs and PDB 7NRC (51) for A-tRNA.

samples that allowed us to obtain the structure with higher resolution (7.7 Å). tRNAs were found to be in A–A and P–P pre-translocation states, and the ribosomal E-site turned out to be empty (Figure 2C). A similar configuration of tRNAs on the ribosome has previously been shown in fungi cells treated with cycloheximide (52).

In both, the averaged tomogram structure and the structure obtained by single particle analysis, the extra electron density was found, consisting of rRNA expansion segment ES27L in the 'tunnel exit' (out) position (53) linked to the top of the ribosome tunnel exit through a protein bridge (Supplementary Figure S3). Since ES27L in this conformation is known to interact with different enzymes including N-terminal acetyltransferases (54) and with proteins of methionine amino peptidase (MetAP) family (55,56) and the additional density was absent in the structure of purified ribosomes (57), we assume that this can be a functional complex participating in the nascent peptide processing. Obtained resolution is not high enough to identify the protein unambiguously, but the size and the position of the density on a ribosome is similar to those of MetAP-2 family proteins (56).

Circular polyribosomes are common in HeLa cell lysate

The definition of the polyribosome topology was based on the topology of the mRNA. The probable pathway of the mRNA chain was traced based on the known positions of mRNA entry and exit sites on the ribosome (58), as well as on an assumption that the mRNA preferably links neighboring ribosomes and that any pseudoknots are not allowed. The topology of a polyribosome was considered circular if the presumable course of the mRNA chain had roughly a ring shape and the distance between ribosomes adjacent along the chain did not exceed the characteristic size of a monosome –30 nm. In all other cases, the polyribosome topology was considered to be linear.

Three hundred and five cytoplasmic polyribosomes were identified in 36 tomograms and four different structural types were defined: topologically circular ring-shaped polyribosomes and topologically linear with more or less regular shapes, namely helices, helix-like structures, and zigzags (Figure 3). For a significant fraction of detected polyribosomes, it was found to be impossible to trace any regular mRNA path which made us classify them as polysomes of indefinite (random) shape (Table 1). Some groups of

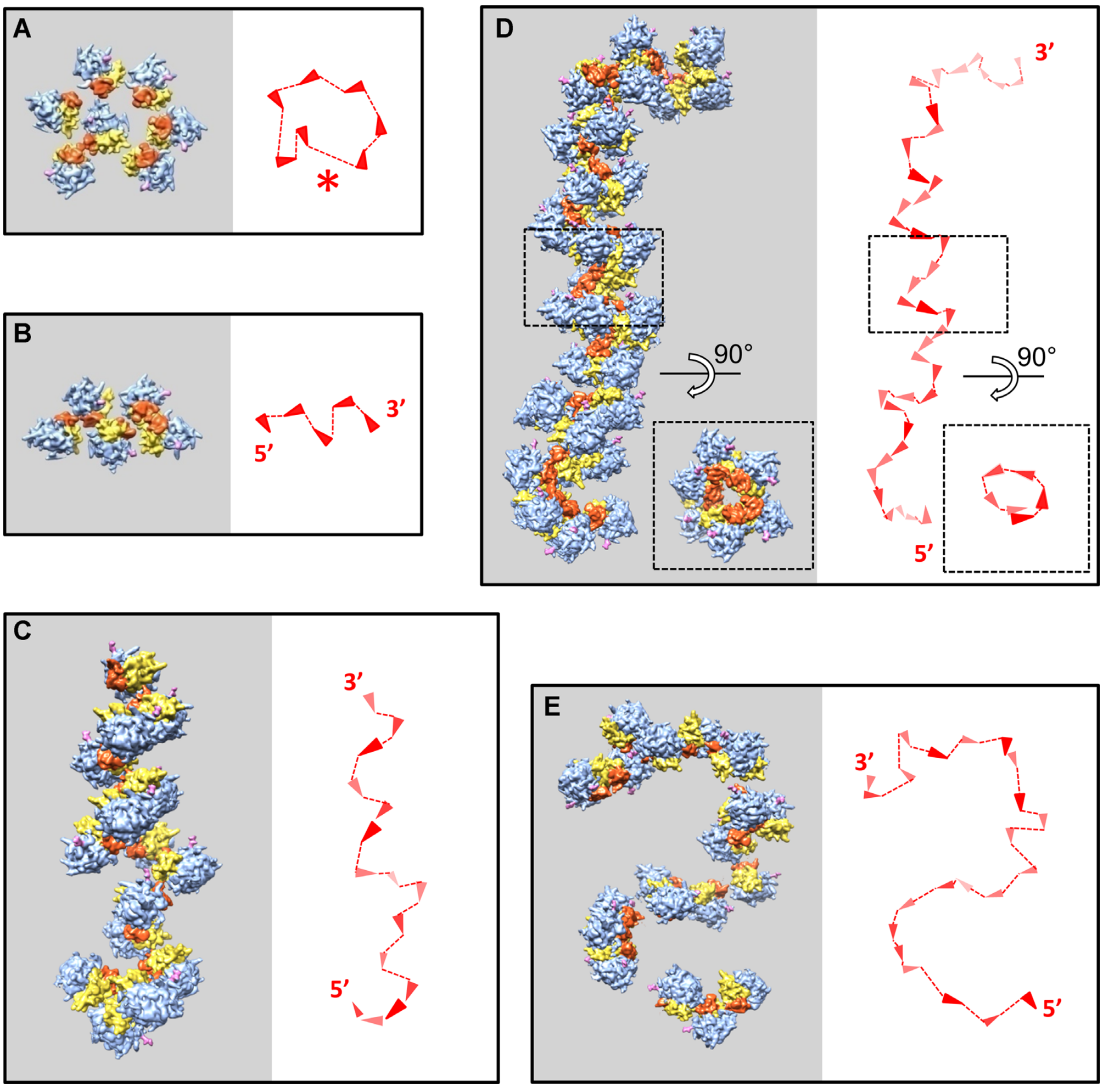

Figure 3. Diversity of polysome organization in HeLa cell lysate. Examples of polyribosomes with circular (**A**), topologically linear zig-zag (**B**), helix-like (**C**), helical (**D**) and randomly shaped (**E**) ribosome arrangements. Copies of the 80S ribosome model acquired from subtomogram analysis were placed into the tomograms at positions and spatial orientations determined by the alignment procedure. Ribosome coloring is the same as in Figure 2A. Right panels: schemes of presumable mRNA pathways evaluated from relative orientation of ribosomes. Arrowheads indicate the direction of the mRNA chain in each ribosome, from the mRNA entry to the exit site.

Table 1. Occurrence of the polyribosomes of different spatial organization in HeLa cell lysate

Type of structural organization	Polyribosome fraction (given type/total)	Polysomal ribosomes fraction (given type/total)
Circular	0.3	0.22
Zig-zag	0.07	0.07
Helix-like	0.03	0.06
3D helix	0.01	0.03
Randomly shaped	0.43	0.41
mRNA path can not be determined	0.16	0.2

ribosomes that could not be combined by one continuous mRNA chain (a single mRNA path could not be determined) were not considered as polysomes. Probably, this could be several polyribosomes stuck together, but it would be impossible to determine is it just aggregates of shorter polyribosomes or some complexes of biological significance.

The structure of circular cellular polyribosomes was found to be identical to that of circular polysomes formed *in vitro* in the wheat germ system (26). In most circular structures, ribosomes are oriented uniformly with small ribosomal subunits directed towards the center of the ring, which attests to an overall circular path of the mRNA chain. Circular polyribosomes of up to six ribosomes size formed basically flat rings, while longer polysomes tended to acquire rather a 3D configuration where the ring principal plane was hard to define (Figure 4). Among all the regular structures circular polyribosomes turned out to be the least loaded – the average loading value was found to be six ribosomes per polysome (Figure 5), while their occurrence in

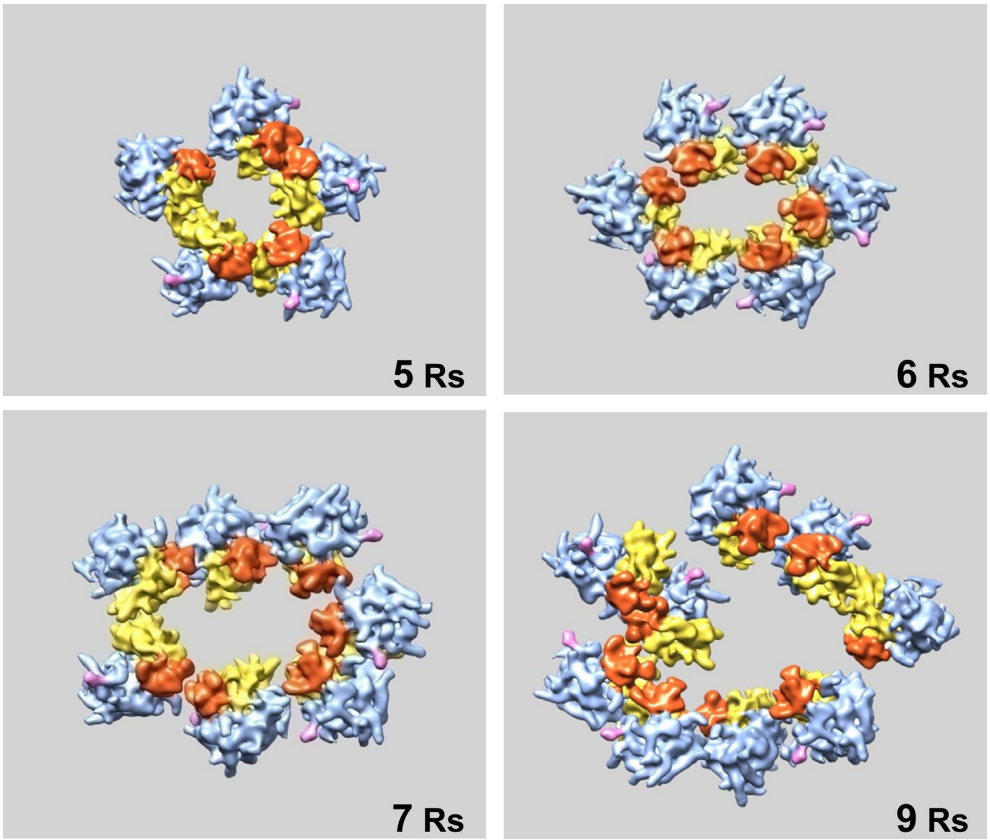

Figure 4. Moderate size polyribosomes of circular topology are common in HeLa cell lysates. Characteristic examples of circular polysomes with 40S subunits looking predominantly inside the ring. The point of view is chosen so that the ribosomes move clockwise along the mRNA chain.

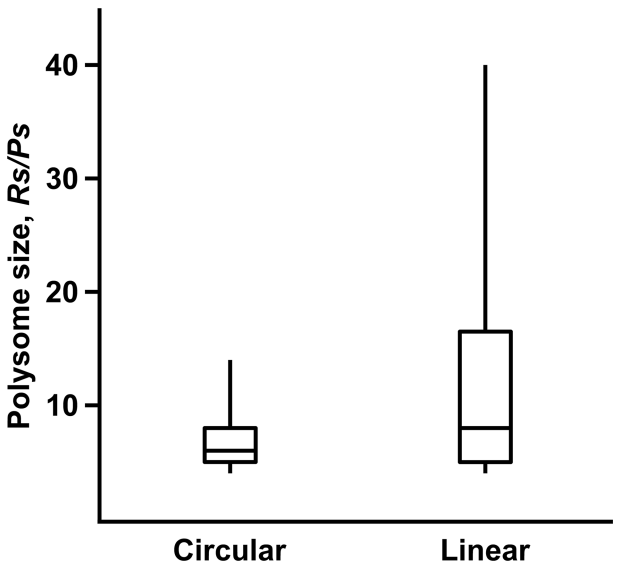

Figure 5. The average ribosome loading value (LV, Rs per mRNA) of circular polyribosomes is significantly less than those of the polysomes of linear topology. The box-plot represents the statistical spread of LV for circular and topologically linear (zig-zag, helical, helix-like and random shape) polyribosomes. The analysis included 93 circular and 164 linear polysomes.

the lysates was fairly high—about 30% of the total (Table 1). In circular polyribosomes, contacts between neighboring ribosomes are not uniform. Probably, that is why this type of polyribosomes was not detected in the *in situ* cryo-ET studies where the definition of polysome structure was based on the analysis of regular inter-ribosomal contacts (30).

Most regular polyribosome structures found in tomograms were left-handed 3D helices with five ribosomes per turn and tight inter-ribosomal contacts along the mRNA chain, resembling four ribosomes per turn helical polysomes which were shown to be almost inactive in a wheat germ cell-free translation system (32,33). The most notable difference, though, is that in the helices formed in HeLa cytoplasm the contacts between consecutive turns are absent, while helical polyribosomes formed *in vitro* have tight contacts not only between neighboring ribosomes but also between ribosomes in adjacent turns. This may indicate that helical polysomes formed *in vivo* are not as tightly packed with ribosomes and retain their translational activity. 3D helices were the most loaded polyribosomes (33 Rs, on average) but represented only a small part of the total number of cellular polysomes (Table 1).

Helix-like polyribosomes found in tomograms were roughly spiral, non-regular structures with loose contacts between ribosomes along the mRNA chain. Surprisingly, they turned out to be right-handed, unlike tightly twisted left-handed 3D helices formed *in vitro* or *in vivo*. In these right-handed polyribosomes each next (downstream) ribosome rotates around longitudinal axis by about 90° clockwise (when viewed in the 5′→3′ direction), and its body, not

head, becomes close to the head of the upstream one. Multiple repetition of such turn results in a right-handed helical structure. Helix-like polyribosomes had an intermediate size (20 Rs, on average) and made up only 3% of polysomes (Table 1). In both helical and helix-like polyribosomes 40S ribosomal subunits were turned inward, to the main axis of the helix, while 60S subunits looked outward.

Zig-zag polysomes of up to 6 ribosomes occurred in a flat double-row form. With increasing size, such polyribosomes acquired features of 3D morphology. It is possible, therefore, that in some cases helical and helix-like polysomes were flattened due to insufficient thickness of the amorphous ice and could be erroneously attributed to zig-zag type. Like helical polyribosomes, zig-zags had an intermediate loading with ribosomes (10 Rs, on average).

Since regular dense inter-ribosomal contacts were not found in the most of HeLa polyribosomes it was impossible to make their classification as it was done in cryo-ET studies of polyribosomes from *E. coli* cell-free system (29) and human glioma cells (30). However, although HeLa cells differ significantly from both these systems, there is general similarity between some inter-ribosomal contacts we observed and 'top-to-top' (the heads of the small subunits are facing each other) and 'top-to-bottom' (the head of one small subunit is facing the opposite part of another) contacts in the helical and zig-zag polyribosome arrangements described previously (29,30).

DISCUSSION

As early as the 1960s, it was shown by conventional TEM methods that in eukaryotic cells ribosomes are packed into polysomes of different shapes (3–13). Cytoplasmic polyribosomes were seen mostly as rings, double rows, and helices (3,8–12,14). In the early studies, double-row polyribosomes were usually interpreted as collapsed rings with two halves of circular polyribosomes brought together (14,27,28). At the same time, such double rows could also represent polysomes with zig-zag or helical path of mRNA chain since they would look similar on TEM pictures of negatively stained samples. Cryo-EM techniques made it possible to distinguish between these interpretations. The modern cryo-EM approach – cryoelectron tomography with subtomogram averaging – allowed to determine the relative orientation of individual ribosomes in polysomes thus identifying the topology of the mRNA chain (26,29–33). Besides, in contrast to classical TEM techniques which involve staining and drying of the sample on the grid, cryo-ET polyribosome specimen is fixed by fast-freezing in conditions close to native. Previously, this approach allowed us to establish that polyribosomes earlier interpreted as double rows (28) may have helical or zig-zag linear mRNA paths (33).

While *in situ* cryo-ET studies of the cell made much progress in recent years, its application to the analysis of polyribosomes encounters serious difficulties, since a high concentration of the ribosomes in a living cell hampers their assignment to specific polysomes (30,36). Here, we avoided this problem by analyzing cryo-EM structures of *in vivo*-formed polyribosomes in diluted mammalian cell lysates. To preserve cellular polyribosomes during the preparation of the lysates cycloheximide was added to the cells before lysis. We checked the presence of tRNAs in the active centers of ribosomes as a criterion of the polysome's translational activity. Although it is known that cycloheximide blocks translation at the translocation stage during elongation, details of the inhibition mechanism are not yet clear. It had previously been assumed that the inhibition of translation occurs when both, tRNA and cycloheximide are located in the ribosomal E-site (59). But later in both structural and functional studies it was shown that tRNA and cycloheximide compete for the binding to the E-site (60,61). Our cryo-ET data revealed the presence of A- and P-site tRNAs in polysomal ribosomes stalled by cycloheximide (in A–A and P–P pre-translocation states, respectively), but the E-site was empty. These data confirm the translationally active state of the polysomal ribosomes in lysates and support the observation that the E-site tRNA is displaced by cycloheximide added in a large proportion. Our results are consistent with the recent high-resolution cryo-EM data on the structure of cycloheximide-stalled translating *Neurospora crassa* ribosomes where two tRNAs in A–A and P–P stated were found, while cycloheximide was located in the empty E-site (52). Apparently, cycloheximide arrests the ribosome in the classical pre-translocation state and prevents its further transition to hybrid pre-translocation conformation (62).

Here, we analyzed structures of 305 cytoplasmic polyribosomes (2976 polysomal ribosomes) and identified different types of polyribosomes with mRNA paths of linear topology, namely zig-zag, helix-like, and helical, as well as ring-like polysomes of circular topology and randomly shaped polyribosomes (Figure 3). In some part of polysomes the inter-ribosomal contacts resembled the common 'top-to-top' (t-t) type previously identified in polyribosomes from prokaryotic (29) and human glioma cells (30). It was assumed that repeated contacts of this type should predominantly lead to the formation of periodic topologically linear structures, like helices or spirals (30). Indeed, we detected polyribosomes of helical and helix-like configurations in the HeLa cell lysate, but the content of these structures was relatively small. This result is consistent with early TEM studies, where the rare occurrence of helical ribosomes in the cytoplasm of eukaryotic cells was first demonstrated (11,12). At the same time, since helices were previously found to be the preferential conformation of polyribosomes in the protrusions of human glioma cells (30) one can not exclude the possibility that a part of polyribosomes lost their helical structure in the course of HeLa cell lysate preparation.

Zig-zag is another polyribosome configuration of linear topology found in the HeLa cell lysate. This type of polyribosome organization also was observed by cryo-ET in both, prokaryotic and eukaryotic systems (29,30), and described as a configuration with alternating 'top-to-top' and 'top-to-bottom' (t-b) inter-ribosomal contacts (29). Although t-t and t-b contacts were found in HeLa zig-zag polyribosomes as well, most of the contacts here were loose and arbitrary.

A large part of the analyzed cytoplasmic polyribosomes possessed a highly variable structure (randomly shaped polyribosomes, 43%), which we could not attribute to any type of regular organization. These data are in agreement

with the results of Brandt et al. who pointed out that polyribosome organization in cells possesses a certain degree of variation (30).

In addition to topologically linear polyribosomes, cryo-ET analysis of HeLa cell lysates revealed polyribosomes with circular mRNA topology, mostly ring-shaped, that made up about one-third of all cellular polysomes. Ring-shaped polyribosomes have previously been repeatedly found in eukaryotic cells using classical TEM methods (3,8–10,14). Here, for the first time, we detected and analyzed by cryo-ET circular cytoplasmic polyribosomes formed *in vivo* and isolated in close-to-native conditions. Interestingly, in recent *in situ* cryo-EM studies of polyribosome organization (30) no clear evidence was found in favor of the closed-loop model of translation (63,64). The authors even concluded that the closed-loop state of mRNA in polyribosomes does not occur in the cell or can be of transient nature (30). Besides, measuring the distance between the 5′ and 3′ ends of long mRNAs in active translating and non-translating mRNP forms lead to the conclusion that the closed-loop structure preferentially forms on non-translating mRNP (65). At the same time, according to biochemical data, the efficiency of closed-loop complex (mRNA ends bound by eIF4E-eIF4G-PABP bridge) formation depends on the length of mRNA (66–68). It was found that mRNAs with short ORF bind close-loop factors (eIF4E-eIF4G-PABP) more efficiently than mRNAs with long ORF, and therefore they are the most highly translated mRNAs in the cells (66–68). Although the lengths of mRNAs involved in polyribosome formation can not be determined with the approach we used, it allowed us to calculate the degree of ribosome loading for the polysomes of different topologies. It turned out that an average circular polyribosome contains fewer ribosomes than linear ones (Figure 5). It may indicate that circular polyribosomes are preferentially generated on mRNAs with relatively short ORF and can further turn to linear when ribosome loading reaches a value too high to maintain circular conformation (more than one ribosome per 100 nts of ORF, (33)). Interestingly, previously it was shown that the formation of circular polyribosomes can be independent of cap structure and the poly(A)-tail (26). It may turn out that, besides protein factors, other components, such as ribosomes themselves, can define polyribosome structure. Because the mRNA path is curved within each ribosome (58) and the ribosomes tend to interact with each other in a more or less regular manner, addition of every downstream ribosome to a polysome bends the mRNA at a certain angle leading to the formation of a circular configuration. This idea has been proposed earlier by several groups (27,69). Alternatively, specific mechanisms of mRNA circularization can exist which are based on elements other than cap structure and poly(A)-tail. Recently, it was reported that methyltransferase METTL3 catalyzing m6A modification in 3′UTR of certain mRNAs interact with h subunit of initiation factor eIF3. The formation of the cap-eIF4-eIF3-METTL3-3′UTR bridge was shown to provide enhancement of translation and formation of densely packed polyribosomes (70). It is most likely that both mechanisms – the formation of a specific bridge between mRNA ends and mRNA bending by ribosomes—can be responsible for the formation of circular polyribosomes.

In summary, cryo-ET analysis of the structural organization of polyribosomes in diluted cell lysates allowed us to detect all forms of cytoplasmic polyribosomes revealed earlier by classical TEM and to describe their topology. This approach can be used in future studies of the relationship between the structure of polyribosomes and the functional state of the cell.

DATA AVAILABILITY

The cryo-EM density maps obtained by subtomogram averaging and single particle analysis have been submitted to the Electron Microscopy Data Bank (EMDB) with accession codes EMD-15008 and EMD-15018, respectively.

SUPPLEMENTARY DATA

Supplementary Data are available at NAR Online.

ACKNOWLEDGEMENTS

We are wholeheartedly grateful to Alexander S. Spirin (RIP), Vladimir A. Shirokov (RIP) and Victor D. Vasiliev (RIP) who initiated this work and helped a lot in early stages. We are also grateful to Elena R. Arutyunyan, Elena A. Chernousova, and Maria V. Dontsova (RIP) for technical assistance. We thank Konstantin S. Vassilenko for fruitful discussions and help in preparation of the manuscript and Alexander G. Myasnikov for helpful advices.

FUNDING

Russian Foundation for Basic Research [16-34-60148]; Russian Science Foundation [19-74-20186 (single particle analysis of eukaryotic ribosomes) to Zh.A.A.]. Funding for open access charge: RFBR [16-34-60148]; RSF [19-74-20186].
Conflict of interest statement. None declared.

REFERENCES

1. Wettstein,F.O., Staehelin,T. and Noll,H. (1963) Ribosomal aggregate engaged in protein synthesis: characterization of the ergosome. *Nature*, **197**, 430–435.
2. Gierer,A. (1963) Function of aggregated reticulocyte ribosomes in protein synthesis. *J. Mol. Biol.*, **6**, 148–IN8.
3. Warner,J.R., Rich,A. and Hall,C.E. (1962) Electron microscope studies of ribosomal clusters synthesizing hemoglobin. *Science*, **138**, 1399–1403.
4. Warner,J.R., Knopf,P.M. and Rich,A. (1963) A multiple ribosomal structure in protein synthesis. *Proc. Natl. Acad. Sci. U.S.A.*, **49**, 122.
5. Rich,A., Warner,J.R. and Goodman,H.M. (1963) The structure and function of polyribosomes. In: *Cold Spring Harbor Symposia on Quantitative Biology*. Cold Spring Harbor Laboratory Press, Vol. **28**, pp. 269–285.
6. Palade,G.E. (1955) A small particulate component of the cytoplasm. *J. Biophys. Biochem. Cytol.*, **1**, 59.
7. Dallner,G., Siekevitz,P. and Palade,G.E. (1966) Biogenesis of endoplasmic reticulum membranes. I. Structural and chemical differentiation in developing rat hepatocyte. *J. Cell. Biol.*, **30**, 73–96.
8. Slayter,H.S., Warner,J.R., Rich,A. and Hall,C.E. (1963) The visualization of polyribosomal structure. *J. Mol. Biol.*, **7**, 652–657.
9. Mathias,P., Williamson,R., Huxley,H.E. and Page,S. (1964) Occurrence and function of polysomes in rabbit reticulocytes. *J. Mol. Biol.*, **9**, 154–167.

10. Shelton,E. and Kuff,E.L. (1966) Substructure and configuration of ribosomes isolated from mammalian cells. *J. Mol. Biol.*, **22**, 23–31.
11. Behnke,O. (1963) Helical arrangement of ribosomes in the cytoplasm of differentiating cells of the small intestine of rat foetuses. *Exp. Cell Res.*, **30**, 597–598.
12. Waddington,C.H. and Perry,M.M. (1963) Helical arrangement of ribosomes in differentiating muscle cells. *Exp. Cell Res.*, **30**, 599–600.
13. Weiss,P. and Grover,N.B. (1968) Helical array of polyribosomes. *Proc. Natl. Acad. Sci. U.S.A.*, **59**, 763.
14. Yazaki,K., Yoshida,T., Wakiyama,M. and Miura,K.I. (2000) Polysomes of eukaryotic cells observed by electron microscopy. *J. Electron Microsc. (Tokyo)*, **49**, 663–668.
15. Philipps,G.R. (1965) Haemoglobin synthesis and polysomes in intact reticulocytes. *Nature*, **205**, 567–570.
16. Adamson,S.D., Howard,G.A. and Herbert,E. (1969) The ribosome cycle in a reconstituted cell-free system from reticulocytes. In: *Cold Spring Harbor Symposia on Quantitative Biology*. Cold Spring Harbor Laboratory Press, Vol. **34**, pp. 547–554.
17. Baglioni,C., Vesco,C.T. and Jacobs-Lorena,M. (1969) The role of ribosomal subunits in mammalian cells. In *Cold Spring Harbor Symposia on Quantitative biology*. Cold Spring Harbor Laboratory Press, Vol. **34**, pp. 555–565.
18. Gallie,D.R. (1991) The cap and poly (A) tail function synergistically to regulate mRNA translational efficiency. *Genes Dev.*, **5**, 2108–2116.
19. Alekhina,O.M., Terenin,I.M., Dmitriev,S.E. and Vassilenko,K.S. (2020) Functional cyclization of eukaryotic mRNAs. *Int. J. Mol. Sci.*, **21**, 1677.
20. Le,H., Tanguay,R.L., Balasta,M.L., Wei,C.C., Browning,K.S., Metz,A.M., Goss,D.J. and Gallie,D.R. (1997) Translation initiation factors eIF-iso4G and eIF-4B interact with the poly (A)-binding protein and increase its RNA binding activity. *J. Biol. Chem.*, **272**, 16247–16255.
21. Tarun,S.Z. Jr and Sachs,A.B. (1996) Association of the yeast poly(A) tail binding protein with translation initiation factor eIF-4G. *EMBO J.*, **15**, 7168–7177.
22. Imataka,H., Gradi,A. and Sonenberg,N. (1998) A newly identified N-terminal amino acid sequence of human eIF4G binds poly (A)-binding protein and functions in poly (A)-dependent translation. *EMBO J.*, **17**, 7480–7489.
23. Borman,A.M., Michel,Y.M., Malnou,C.E. and Kean,K.M. (2002) Free poly (A) stimulates capped mRNA translation in vitro through the eIF4G-poly (A)-binding protein interaction. *J. Biol. Chem.*, **277**, 36818–36824.
24. Wells,S.E., Hillner,P.E., Vale,R.D. and Sachs,A.B. (1998) Circularization of mRNA by eukaryotic translation initiation factors. *Mol. Cell*, **2**, 135–140.
25. Archer,S.K., Shirokikh,N.E., Hallwirth,C.V., Beilharz,T.H. and Preiss,T. (2015) Probing the closed-loop model of mRNA translation in living cells. *RNA Biol.*, **12**, 248–254.
26. Afonina,Z.A., Myasnikov,A.G., Shirokov,V.A., Klaholz,B.P. and Spirin,A.S. (2014) Formation of circular polyribosomes on eukaryotic mRNA without cap-structure and poly (A)-tail: a cryo electron tomography study. *Nucleic Acids Res.*, **42**, 9461–9469.
27. Madin,K., Sawasaki,T., Kamura,N., Takai,K., Ogasawara,T., Yazaki,K., Takei,T., Miura,K. and Endo,Y. (2004) Formation of circular polyribosomes in wheat germ cell-free protein synthesis system. *FEBS Lett.*, **562**, 155–159.
28. Kopeina,G.S., Afonina,Z.A., Gromova,K.V., Shirokov,V.A., Vasiliev,V.D. and Spirin,A.S. (2008) Step-wise formation of eukaryotic double-row polyribosomes and circular translation of polysomal mRNA. *Nucleic Acids Res.*, **36**, 2476–2488.
29. Brandt,F., Etchells,S.A., Ortiz,J.O., Elcock,A.H., Hartl,F.U. and Baumeister,W. (2009) The native 3D organization of bacterial polysomes. *Cell*, **136**, 261–271.
30. Brandt,F., Carlson,L.A., F. Hartl,U., Baumeister,W. and Grünewald,K. (2010) The three-dimensional organization of polyribosomes in intact human cells. *Mol. Cell.*, **39**, 560–569.
31. Afonina,Z., Myasnikov,A.G., Khabibullina,N.F., Belorusova,A.Y., Menetret,J.F., Vasiliev,V.D., Klaholz,B.P., Shirokov,V.A. and Spirin,A.S. (2013) Topology of mRNA chain in isolated eukaryotic double-row polyribosomes. *Biochemistry (Mosc.)*, **78**, 445–454.
32. Myasnikov,A.G., Afonina,Z.A., Ménétret,J.F., Shirokov,V.A., Spirin,A.S. and Klaholz,B.P. (2014) The molecular structure of the left-handed supra-molecular helix of eukaryotic polyribosomes. *Nat. Commun.*, **5**, 5294.
33. Afonina,Z.A., Myasnikov,A.G., Shirokov,V.A., Klaholz,B.P. and Spirin,A.S. (2015) Conformation transitions of eukaryotic polyribosomes during multi-round translation. *Nucleic Acids Res.*, **43**, 618–628.
34. Khoshouei,M., Pfeffer,S., Baumeister,W., Förster,F. and Danev,R. (2017) Subtomogram analysis using the volta phase plate. *J. Struct. Biol.*, **197**, 94–101.
35. Nedozralova,H., Basnet,N., Ibiricu,I., Bodakuntla,S., Biertümpfel,C. and Mizuno,N. (2022). In situ cryo-electron tomography reveals local cellular machineries for axon branch development. *J. Cell Biol.*, **221**, e202106086.
36. Jiang,W., Wagner,J., Du,W., Plitzko,J., Baumeister,W., Beck,F. and Guo,Q. (2022). A transformation clustering algorithm and its application in polyribosomes structural profiling. *Nucleic Acids Res.*, **50**, 9001–9011.
37. Kremer,J.R., Mastronarde,D.N. and McIntosh,J.R. (1996) Computer visualization of three-dimensional image data using IMOD. *J. Struct. Biol.*, **116**, 71–76.
38. Radermacher,M. (2007) Weighted back-projection methods. In: *Electron Tomography*. Springer, pp. 245–273.
39. Kimanius,D., Forsberg,B.O., Scheres,S.H. and Lindahl,E. (2016) Accelerated cryo-EM structure determination with parallelisation using GPUs in RELION-2. *Elife*, **5**, e18722.
40. Bharat,T.A. and Scheres,S.H. (2016) Resolving macromolecular structures from electron cryo-tomography data using subtomogram averaging in RELION. *Nat. Protoc.*, **11**, 2054–2065.
41. Rohou,A. and Grigorieff,N. (2015) CTFFIND4: fast and accurate defocus estimation from electron micrographs. *J. Struct. Biol.*, **192**, 216–221.
42. Van Heel,M. and Schatz,M. (2005). Fourier shell correlation threshold criteria. *J. Struct. Biol.*, **151**, 250–262.
43. Rosenthal,P.B. and Henderson,R. (2003). Optimal determination of particle orientation, absolute hand, and contrast loss in single-particle electron cryomicroscopy. *J. Mol. Biol.*, **333**, 721–745.
44. Pettersen,E.F., Goddard,T.D., Huang,C.C., Couch,G.S., Greenblatt,D.M., Meng,E.C. and Ferrin,T.E. (2004) UCSF Chimera—a visualization system for exploratory research and analysis. *J. Comput. Chem.*, **25**, 1605–1612.
45. Tegunov,D. and Cramer,P. (2019) Real-time cryo-electron microscopy data preprocessing with warp. *Nat. Methods*, **16**, 1146–1152.
46. Punjani,A., Rubinstein,J.L., Fleet,D.J. and Brubaker,M.A. (2017) cryoSPARC: algorithms for rapid unsupervised cryo-EM structure determination. *Nat. Methods*, **14**, 290–296.
47. Johannes,G. and Sarnow,P. (1998) Cap-independent polysomal association of natural mRNAs encoding c-myc, BiP, and eIF4G conferred by internal ribosome entry sites. *RNA*, **4**, 1500–1513.
48. Thompson,R.F., Walker,M., Siebert,C.A., Muench,S.P. and Ranson,N.A. (2016) An introduction to sample preparation and imaging by cryo-electron microscopy for structural biology. *Methods*, **100**, 3–15.
49. Briggs,J.A. (2013) Structural biology in situ—the potential of subtomogram averaging. *Curr. Opin. Struct. Biol.*, **23**, 261–267.
50. Behrmann,E., Loerke,J., Budkevich,T.V., Yamamoto,K., Schmidt,A., Penczek,P.A., Vos,M.R., Bürger,J., Mielke,T., Scheerer,P. *et al.* (2015) Structural snapshots of actively translating human ribosomes. *Cell*, **161**, 845–857.
51. Pochopien,A.A., Beckert,B., Kasvandik,S., Berninghausen,O., Beckmann,R., Tenson,T. and Wilson,D.N. (2021) Structure of gcn1 bound to stalled and colliding 80S ribosomes. *Proc. Natl. Acad. Sci. U.S.A.*, **118**, e2022756118.
52. Shen,L., Su,Z., Yang,K., Wu,C., Becker,T., Bell-Pedersen,D., Zhang,J. and Sachs,M.S. (2021) Structure of the translating neurospora ribosome arrested by cycloheximide. *Proc. Natl. Acad. Sci. U.S.A.*, **118**, e2111862118.
53. Armache,J.P., Jarasch,A., Anger,A.M., Villa,E., Becker,T., Bhushan,S., Jossinet,F., Habeck,M., Dindar,G., Franckenberg,S. *et al.* (2010) Cryo-EM structure and rRNA model of a translating eukaryotic 80S ribosome at 5.5-Å resolution. *Proc. Natl. Acad. Sci. U.S.A.*, **107**, 19748–19753.
54. Knorr,A.G., Schmidt,C., Tesina,P., Berninghausen,O., Becker,T., Beatrix,B. and Beckmann,R. (2019). Ribosome–NatA architecture

reveals that rRNA expansion segments coordinate N-terminal acetylation. *Nat. Struct. Mol. Biol.*, **26**, 35–39.
55. Fujii,K., Susanto,T.T., Saurabh,S. and Barna,M. (2018). Decoding the function of expansion segments in ribosomes. *Mol. Cell*, **72**, 1013–1020.
56. Wild,K., Aleksić,M., Lapouge,K., Juaire,K.D., Flemming,D., Pfeffer,S. and Sinning,I. (2020) MetAP-like ebp1 occupies the human ribosomal tunnel exit and recruits flexible rRNA expansion segments. *Nat. Commun.*, **11**, 776.
57. Khatter,H., Myasnikov,A.G., Natchiar,S.K. and Klaholz,B.P. (2015) Structure of the human 80S ribosome. *Nature*, **520**, 640–645.
58. Yusupova,G.Z., Yusupov,M.M., Cate,J.H.D. and Noller,H.F. (2001) The path of messenger RNA through the ribosome. *Cell*, **106**, 233–241.
59. Schneider-Poetsch,T., Ju,J., Eyler,D.E., Dang,Y., Bhat,S., Merrick,W.C., Green,R., Shen,B. and Liu,J.O. (2010) Inhibition of eukaryotic translation elongation by cycloheximide and lactimidomycin. *Nat. Chem. Biol.*, **6**, 209–217.
60. Garreau de Loubresse,N., Prokhorova,I., Holtkamp,W., Rodnina,M.V., Yusupova,G. and Yusupov,M. (2014) Structural basis for the inhibition of the eukaryotic ribosome. *Nature*, **513**, 517–522.
61. Myasnikov,A.G., Kundhavai Natchiar,S., Nebout,M., Hazemann,I., Imbert,V., Khatter,H., Peyron,J-F. and Klaholz,B.P. (2016). Structure–function insights reveal the human ribosome as a cancer target for antibiotics. *Nat. Commun.*, **7**, 12856.
62. Bhaskar,V., Graff-Meyer,A., Schenk,A.D., Cavadini,S., von Loeffelholz,O., Natchiar,S.K., Artus-Revel,C.G., Hotz,H.R., Bretones,G., Klaholz,B.P. *et al.* (2020) Dynamics of uS19 C-terminal tail during the translation elongation cycle in human ribosomes. *Cell Rep.*, **31**, 107473.
63. Jacobson,A. (1996) Poly (A) metabolism and translation: the closed-loop model. In: Hershey,J.W.B., Mathews,M.B. and Sonenberg,N. (eds). *Translational Control*. Cold Spring Harbor Laboratory Press, NY, pp. 451–480.
64. Preiss,T. and Hentze,M.W. (1999) From factors to mechanisms: translation and translational control in eukaryotes. *Curr. Opin. Genet. Dev.*, **9**, 515–521.
65. Khong,A. and Parker,R. (2018) mRNP architecture in translating and stress conditions reveals an ordered pathway of mRNP compaction. *J. Cell Biol.*, **217**, 4124–4140.
66. Amrani,N., Ghosh,S., Mangus,D.A. and Jacobson,A. (2008) Translation factors promote the formation of two states of the closed-loop mRNP. *Nature*, **453**, 1276–1280.
67. Thompson,M.K., Rojas-Duran,M.F., Gangaramani,P. and Gilbert,W.V. (2016) The ribosomal protein asc1/rack1 is required for efficient translation of short mRNAs. *Elife*, **5**, e11154.
68. Thompson,M.K. and Gilbert,W.V. (2017) mRNA length-sensing in eukaryotic translation: reconsidering the 'closed loop' and its implications for translational control. *Curr. Genet.*, **63**, 613–620.
69. Christensen,A.K. and Bourne,C.M. (1999) Shape of large bound polysomes in cultured fibroblasts and thyroid epithelial cells. *Anat. Rec.*, **255**, 116–129.
70. Choe,J., Lin,S., Zhang,W., Liu,Q., Wang,L., Ramirez-Moya,J., Du,P., Kim,W., Tang,S., Sliz,P. *et al.* (2018) mRNA circularization by METTL3–eIF3h enhances translation and promotes oncogenesis. *Nature*, **561**, 556–560.